ACS EARTH AND SPACE CHEMISTRY

http://pubs.acs.org/journal/aesccq

Article

Phase State and Thermodynamic Properties of Proxy Sea Spray Aerosol Interfaces Derived from Temperature-Dependent Equilibrium Spreading Pressure

Mickey M. Rogers, Maria G. Vazquez de Vasquez, Jennifer F. Neal, Mia M. Zerkle, Brittany M. Shook, and Heather C. Allen*

Cite This: https://doi.org/10.1021/acsearthspacechem.2c00063

Read Online

ACCESS | Metrics & More | Article Recommendations | Supporting Information

ABSTRACT: To gain global understanding of the complex interactions marine organics participate in at the surface of sea spray aerosols (SSAs), thermodynamic parameters are needed as inputs for atmospheric models. Traditional surface studies use Langmuir films that exist in pseudoequilibrium and require assumptions to obtain thermodynamic properties. To address these challenges, we have developed a new application for equilibrium spreading pressure (ESP), an experimental value based on the true thermodynamic equilibrium between a film and its solid form at the aqueous interface. By changing the equilibrium phase state of a marine relevant palmitic acid/palmitate (PA) monolayer as a function of temperature (7.0−20.2 °C) and sodium chloride concentration (1−1000 mM), we can experimentally capture the thermodynamic values of three-dimensional (3D) solid to two-dimensional (2D) monolayer spreading. Cooler temperatures present more unfavorable and disordered conditions for spreading PA into a 2D film. However, the addition of NaCl to the solution does not follow a monotonical trend in thermodynamic values, exhibited by an anomalous 100 mM NaCl condition, which is ∼20 and ∼35% more enthalpically favorable than 10 and 1000 mM NaCl, respectively. Our results represent some of the first thermodynamic data for spreading PA from 3D solid to 2D film given atmospheric conditions and the first study to utilize ESP to determine the thermodynamic properties of PA−Na^+ interactions. Our true equilibrium-based approach helps to inform on the 3D to 2D phase-state transition of organic coatings, presenting an essential input for climate models and global understanding of SSA interfaces.

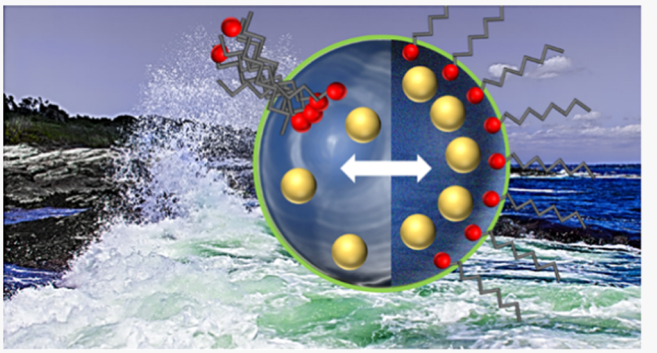

KEYWORDS: *air−seawater interface, carboxylate interaction, equilibrium spreading pressure, phase state, sea spray aerosol*

INTRODUCTION

Sea spray aerosols (SSAs) present highly dynamic microenvironments in which their interfacial properties are strongly driven by chemical and physical interactions such as carboxylate−metal binding,[1,2] acid−base equilibrium,[3−5] and ion hydration.[6−8] Each of these parameters unlocks important thermodynamic inputs for global climate models, which provide better insights into atmospheric phenomena like ice nucleation and cold cloud formation. The key to unraveling these thermodynamically driven interactions is equilibrium-based measurements and calculations.[9,10] Herein, we use equilibrium spreading pressure (ESP) measurements to calculate the thermodynamic equilibrium between the three-dimensional (3D) solid phase and a two-dimensional (2D) film of a fatty acid monolayer to inform on the interfacial chemistry of SSA organic coatings.[11]

Conventional Langmuir techniques such as surface pressure-area (Π-A) isotherms measure monolayers in a pseudoequilibrium in which barrier compression forces the monolayer into a specific phase state.[12] Conversely, ESP measurements maintain the monolayer at a true equilibrium that remains constant over time. The temperature[13] and composition of the aqueous solution (i.e., the addition of metal ions such as Ca^{2+}, Na^+)[14] have been found to drive the ESP value, consistent with shifting equilibriums due to interactions. As SSA age, they are exposed to cooling temperature and fluctuations in relative humidity, changing the concentration of ions present in their aqueous core. ESP measurements have been taken of various surfactants including fatty acids,[15] fatty alcohols,[16] phospho-

Received: March 2, 2022
Revised: April 19, 2022
Accepted: April 25, 2022

lipids,[17] and proteins.[18] In the past, ESP has been notably used to describe the thermochemical properties of surfactants at ranging temperatures, particularly near their melting points.[15−17,19] More recently, the influence of ESP on ice nucleation has been established.[20−22] However, a combination of atmospheric conditions such as temperature and sodium concentration has yet to be considered together when calculating ESP-derived thermodynamics.

While ESP studies have demonstrated historic significance in defining the thermodynamic properties of spreading organics from 3D solid to 2D films, ESP has yet to be extended to calculating the thermodynamic equilibrium of carboxylate−metal interactions for SSA systems. Our work marks the revived importance of ESP studies for understanding organic coating phase state under atmospheric conditions and determines the thermodynamic preference for Na^+ to interact with a palmitic acid/palmitate (PA) monolayer, as shown in Figure 1. Carboxylate−metal interactions under oceanic and

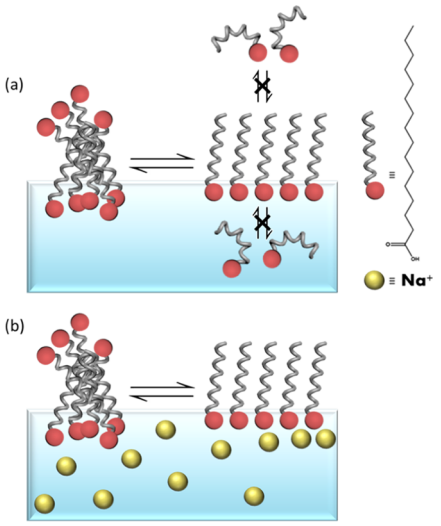

Figure 1. Schematic representation of equilibrium spreading pressure where (a) the thermodynamic equilibrium of spreading is between the 3D solid phase and the 2D monolayer phase and (b) the proposed mechanism of thermodynamic equilibrium of metal interactions between the 2D monolayer of PA and Na^+.

atmospheric conditions have been well documented in the literature using various spectroscopic techniques.[1−3,23] Exposure to high concentrations of NaCl drives the interfacial equilibrium for certain semisoluble acids, demonstrating a need to expand upon Na^+ studies, such as their thermodynamically driven interactions, at SSA interfaces.[3] However, the thermodynamic properties of these carboxylate−metal interactions persist as nontrivial measurements. Using our ESP approach for determining the true equilibrium state of the PA−Na^+ interaction, we can calculate the thermodynamic properties of a carboxylate−metal system.

Our results show the quantitative thermodynamic analysis of PA−Na^+ interactions at the air−water interface, based on relevantly low temperatures to further our molecular understanding of organic coatings on SSAs under atmospheric conditions.[15,16] Overall, warmer temperatures consistently present more favorable and ordered conditions for spreading PA from the 3D to 2D phase state. Upon the addition of 100 mM NaCl, we observe an anomalous condition that pushes the equilibrium of spreading in favor of the 2D PA monolayer phase, being ∼20 and ∼35% more enthalpically favorable than 10 and 1000 mM NaCl solutions, respectively. Results from our study provide insights into the physicochemical processes for modeling SSA systems, providing new and essential considerations of ionic interactions with organic coatings.

METHODS

Chemicals and Sample Preparation. Palmitic acid ($C_{16}H_{32}O_2$, ≥99%, Sigma-Aldrich) was purchased in high purity and used without further purification. Palmitic acid was either ground into a finer powder using a mortar and pestle to ensure uniform particle size for equilibrium spreading pressure studies or dissolved in chloroform (HPLC Grade, Fisher Scientific) at a concentration of 1.86 mM for surface pressure-area (Π-A) isotherms. Sodium chloride (trace metal grade, 99.999%, ACROS and Sigma-Aldrich) was baked at 650 °C for >6 h prior to use. Sodium chloride solutions with concentrations from 1, 10, 100, and 1000 mM were prepared with ultrapure water with a resistivity of 18.2 MΩ·cm (Milli-Q Advantage A10) and allowed time to acidify by atmospheric CO_2 to pH 5.6 ± 0.7.

Measurements were also taken with ethylenediaminetetraacetic acid (EDTA) (99.995%, Sigma-Aldrich) to ensure that the trace metal grade sodium chloride was sufficiently void of heavy metal contaminates, as shown in Figure S1. A representative low concentration of sodium chloride with 1 mM NaCl and 1 μM EDTA was prepared. The solution was then pH adjusted using NaOH to account for the lowering in pH due to the acidity of the EDTA species. The inclusion of EDTA will bind to any other metals that could be in the NaCl solution. As the 1 mM NaCl measurement at 20.2 °C remains constant with and without EDTA, our trace metal solutions were free of other metal contaminants that could influence our measurements. No unexpected or unusually high safety hazards were encountered in chemical preparation.

Equilibrium Spreading Pressure. A Teflon Langmuir trough (KSV Medium, KN 2002) was thoroughly cleaned with reagent alcohol, and temperature controlled by a water circulator attached to a temperature control system (Julabo Easy Temp F12-ed). The trough has a network of hollow internal metal coils that circulate a water−ethylene glycol mixture. The water−ethylene glycol mixture was circulated throughout the coil system to maintain the temperature of the solutions. The solution temperature was adjusted to temperatures of 7.0 ± 1.0, 12.9 ± 1.0, 16.3 ± 1.0, and 20.2 ± 1.0 °C and was monitored constantly using a clean temperature probe inserted into the aqueous solution. The solution temperature was recorded throughout the experiment and did not fluctuate more than 1 °C. Furthermore, the trough was encased inside a plexiglass box to prevent dust and other particles from contaminating the surface or disrupting the surface pressure measurements. Approximately 100 mg of ground palmitic acid, measured and recorded on an analytical balance for each trial, was sprinkled over the solution of interest using weigh paper. Equilibrium spreading pressure (ESP) was measured by the Wilhelmy plate method using filter paper plates (Ashless, grade 41, Whatman). The time it took to reach the ESP varied between trials, so the data shown are scaled so the surface pressure liftoff is consistent among trials. All data was processed using Origin software (OriginLab, Northampton, MA) using the average and EXPGROW2 fitting.

Surface Pressure-Area (Π-A) Isotherms. Surface pressure (Π) was measured in triplicate using a custom Teflon

https://doi.org/10.1021/acsearthspacechem.2c00063
ACS Earth Space Chem. XXXX, XXX, XXX−XXX

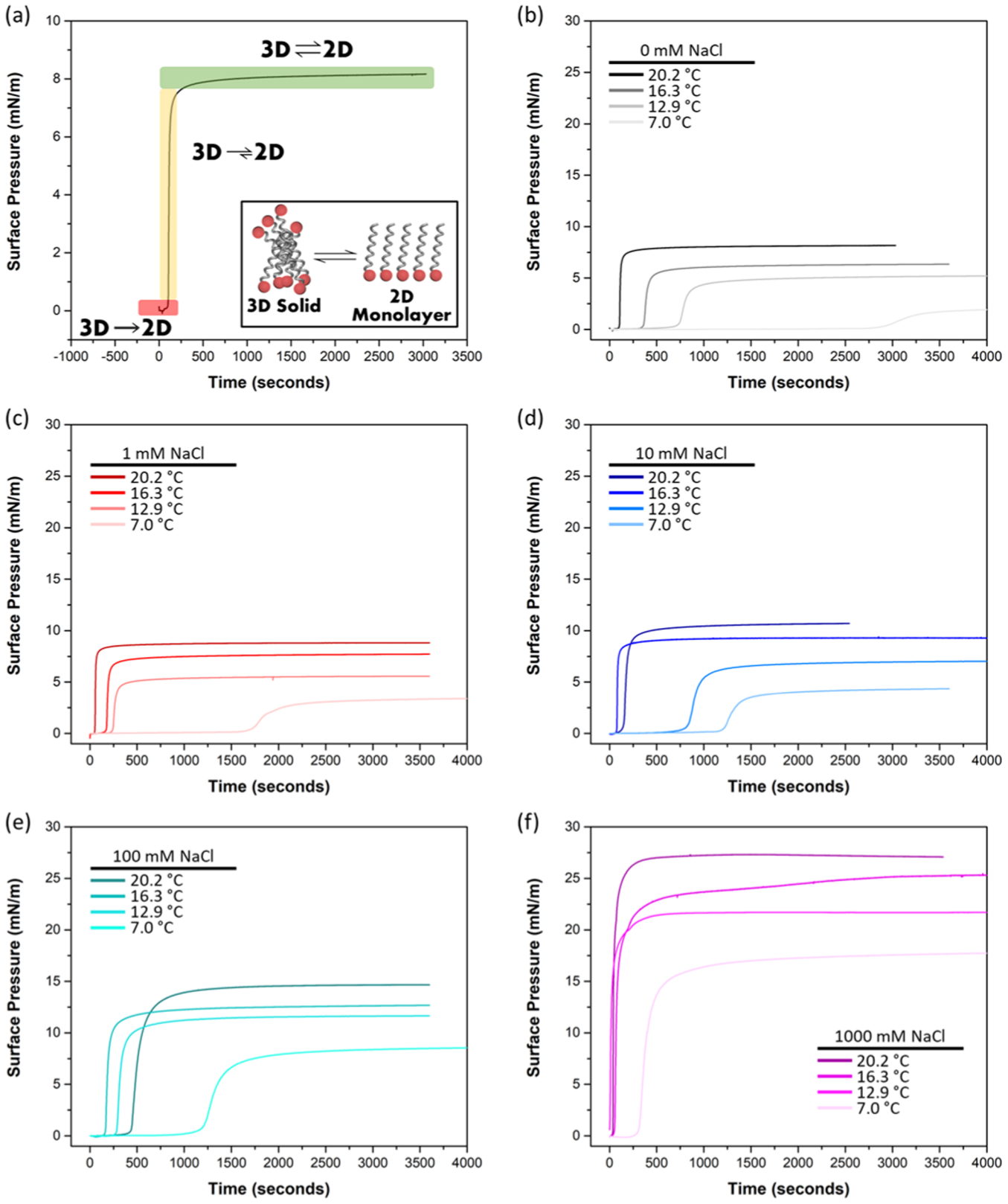

Figure 2. Equilibrium spreading pressure (π_e) (a) schematic of proposed equilibria for PA 3D to 2D phase-state transition and (b) measurements of PA on water (black), (c) 1 mM NaCl (red), (d) 10 mM NaCl (blue), (e) 100 mM NaCl (teal), and (f) 1000 mM NaCl (pink) solutions at varying temperatures. As the temperature of a given chemical system increases, the ESP value increases linearly. Increasing the temperature pushes the equilibrium in favor of the 2D PA monolayer phase.

Langmuir trough (KSV NIMA, area 144.5 cm^2) by the Wilhelmy plate method (platinum, 39.240 mm perimeter). The trough was thoroughly cleaned with reagent alcohol, and the plate was cleaned by Milli-Q water and reagent alcohol and then flamed dry prior to use. A water circulator (ISOTEMP 4100C, Fisher Scientific, Inc.) was used to control the

https://doi.org/10.1021/acsearthspacechem.2c00063
ACS Earth Space Chem. XXXX, XXX, XXX−XXX

temperature of the solution in the trough at constant temperatures of 7.0 ± 0.3, 12.9 ± 0.3, 16.3 ± 0.3, and 20.2 ± 0.3 °C and was monitored constantly using a clean temperature probe inserted into the aqueous solution. The setup was housed in a plexiglass box to prevent exposure to dust and other particulate matter. The Langmuir trough was filled with a solution of interest, palmitic acid solution was spread dropwise onto the aqueous surface using a microsyringe (50 μL, Hamilton), and then measurements began after a 10 min delay for solvent evaporation. The Π was monitored over time as Delrin barriers (KSV NIMA) were compressed symmetrically at a rate 5 mm/min/barrier. The plots are shown as the mean of at least three trials, and error bars are shown as shaded regions on the plot and represent one standard deviation above and below the mean. All data was processed using Origin software (OriginLab, Northampton, MA) using the average.

RESULTS AND DISCUSSION

Temperature and Sodium Drive Phase-State Equilibrium for Palmitic Acid Monolayers. We explore the critical role that both temperature, ranging from 7.0 to 20.2 °C, and sodium concentration, ranging from 1 to 1000 mM NaCl, play in driving the equilibrium spreading pressure (ESP) of palmitic acid/palmitate (PA) monolayers. Figure 2 shows our ESP results as a function of temperature and sodium concentration.

The ESP schematic in Figure 2a illustrates the equilibrium between the 3D solid of PA to the 2D monolayer. Equilibrium is achieved at a metastable state, which corresponds to the maximum surface pressure. Any loss of the 2D PA monolayer into the solution would shift the equilibrium from the 3D solid phase to the 2D monolayer to counteract monolayer depletion into the bulk. If the rate of loss from the 2D monolayer phase is larger than the rate needed to re-establish the 3D−2D equilibrium, then the surface pressure cannot be maintained and a decrease in surface pressure will be observed.[14] We do not observe a decrease in surface pressure over time, suggesting that the equilibrium is achieved and maintained in the metastable state. Our results in Figure 2 reveal consistent maintenance of the 3D−2D equilibrium for all temperature ranges and NaCl concentrations.

It is evident that temperature affects the ESP values, as shown in Figure 2b, which corresponds to the measurements of PA on pure water. As the temperature is decreased, the ESP value decreases, as well, going from ∼ 8 to ∼2.5 mN/m. At lower temperatures, we also observe a prolonged equilibration time for the 3D solid of PA to spread into a 2D monolayer, suggesting that this process is thermodynamically unfavored at cooler temperatures. Figure 2c−f shows the influence of NaCl on the ESP at isothermal conditions. We observe that the addition of NaCl increases the ESP value at each temperature compared to pure water. These results suggest that NaCl induces a preference toward the 2D PA monolayer phase state.

Literature has shown similar trends in temperature dependence, where ESP increases with warmer temperatures.[24] More Na^+ available to bind, electrostatically interact with, or intercalate between the carboxylate headgroups of the PA monolayer creates a more stabilized interface, which increases the ESP. Previous literature supports these findings.[20,25−27] Figure 3 summarizes the trends in ESP, where warmest temperatures and highest NaCl concentrations induce the largest ESPs.

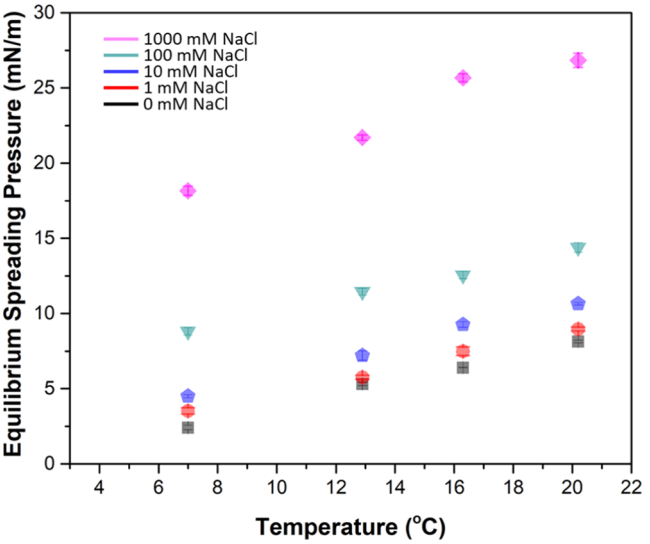

Figure 3. Equilibrium spreading pressures (π_e) of PA on 1000 mM NaCl (pink), 100 mM NaCl (teal), 10 mM NaCl (blue), 1 mM NaCl (red), and water (black) solutions at varying temperatures to determine $\frac{d\pi_e}{dT}$, the slope of the ESP values on a NaCl solution. The error bars represent one standard deviation of the measurements (note the error bars fall within the size of the symbols).

We use Langmuir surface pressure-area (Π-A) isotherms to determine the mean molecular area (MMA) that corresponds to the ESP values in Figures 3 and S2. Generally, the presence of NaCl compresses the liftoff point in warmer conditions, similar to previous findings.[28] Every ESP value for water, 1, 10, and 100 mM NaCl at each temperature corresponds to a MMA within the tilted condensed (TC) phase of the PA Π-A isotherms, as shown in Figure 4, likely due to intercalation or Na^+ interaction at the interface.[3] However, the 1 M NaCl ESP values correspond to MMAs within the untilted condensed (UC) phase due to the lower surface pressure transition from the TC to UC phase. In Figure 4a−c, the 1 M NaCl Π-A isotherms lift off at the lowest MMA and remain most compressed in their TC phase. Upon transition from the TC to UC phase, the 1 M NaCl Π-A isotherms undergo an expansion which is maintained to the highest surface pressures observed, as shown prior.[29] This expansion at significantly higher surface pressures is likely a result of the long-range electrostatic interactions of Na^+ with the deprotonated headgroups in the PA monolayer, consistent with another study.[30] The higher charge density of 1 M NaCl at the interface helps to stabilize the UC phase for higher surface pressures before collapse. While this trend is observed in the 20.2, 16.3, and 12.9 °C Π-A isotherms, the 7.0 °C study, shown in Figure 4d, maintains expansion for the entirety of the 1 M NaCl study, likely due to the complex interplay of high Na^+ in solution at low temperatures. Across all NaCl systems, the 7.0 °C Π-A isotherms show expansion in the TC phase compared to the other temperatures, supporting the break in trend for the 1 M NaCl study at 7.0 °C.

We see consistent trends in the collapse phase, as depicted in Figures 4 and S3, across NaCl concentrations within a measured temperature. Each temperature studied maintains the following order of highest to lowest collapse surface pressure: 1000, 100, 10, and 1 mM NaCl. Additionally, the postcollapse equilibrium achieved after the collapse maintains the same order of highest to lowest surface pressure,

https://doi.org/10.1021/acsearthspacechem.2c00063
ACS Earth Space Chem. XXXX, XXX, XXX−XXX

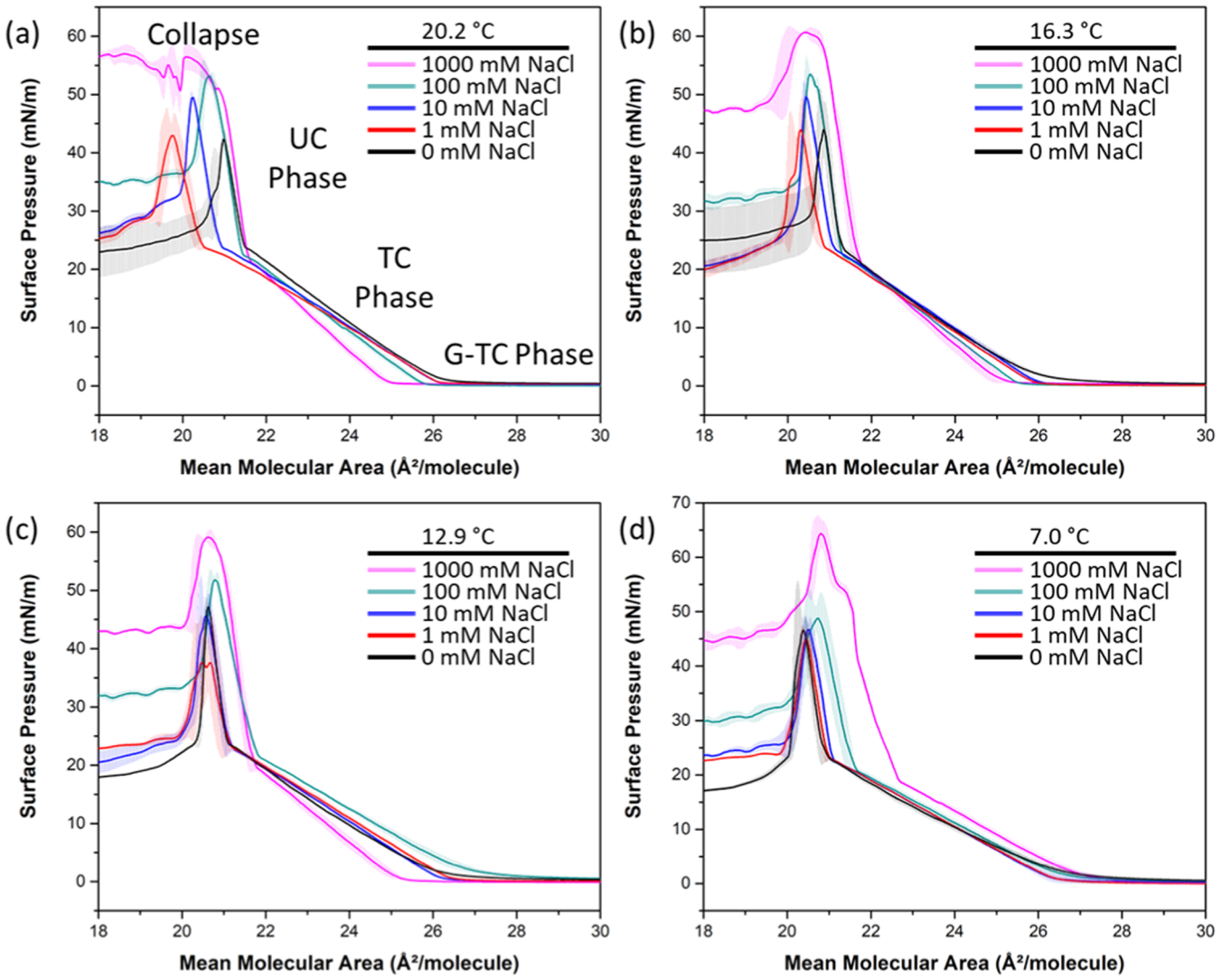

Figure 4. Surface pressure-area (Π-A) isotherms of PA on 1000 mM NaCl (pink), 100 mM NaCl (teal), 10 mM NaCl (blue), 1 mM NaCl (red), and water (black) subphases at (a) 20.2 °C, (b) 16.3 °C, (c) 12.9 °C, and (d) 7.0 °C for determining the MMA at corresponding ESP to calculate thermodynamic values. The shaded regions represent one standard deviation of the measurements.

respectively, and similarly to other studies.[31−33] Work by Lipp et al. supports our findings on Na^+ maintaining the UC phase at higher surface pressures, yielding a higher surface pressure at collapse.[28] For the two warmer conditions, 20.2 and 16.3 °C, all concentrations of NaCl experience collapse at higher surface pressures than water. The increased ionic strength of the NaCl solution compared to pure water leads to a relatively high surface charge density, preventing the formation of bulk collapse structures that would otherwise experience electrostatic repulsion with deprotonated PA molecules remaining in the monolayer. As well, Coulombic repulsion between the carboxylate moieties of the PA or the contact ion pair formation between the carboxylate and Na^+ could explain the trend in collapse phase behavior.[29,34]

Thermodynamic Properties of Spreading Palmitic Acid from a 3D Solid to 2D Film on Sodium Chloride Subphases at Varying Temperatures. The thermodynamic properties of spreading from a 3D solid to a 2D film depend on the molecular structure of a fatty acid such as its headgroup or chain length and its potential for lipid−lipid interactions compared to lipid−water interactions.[15] The solubility of surfactants as well as dispersion interactions among neighboring surfactants can influence the thermodynamic properties of spreading from a 3D solid to a 2D film. The energy required to break from the initial 3D solid material deposited on the surface and spread into the 2D monolayer form also determines the equilibrium. More specifically, the role of temperature pushes the energetics in favor of the 2D monolayer phase state,[15,17,24,28,35] but the influence of aqueous Na^+ remains understudied for calculating and interpreting the thermodynamic properties of spreading from 3D to 2D phase-state transition.

Experimentally obtained ESP values can be coupled with Π-A isotherms to simplify otherwise complicated calculations for thermodynamic properties, shown in Figure S2.[15,16,24,36] Using three equations adapted from the Clausius−Clapeyron equation and presented by Jalal et al., we can calculate and discern changes in enthalpy (ΔH_s), entropy (ΔS_s), and Gibb's free energy (ΔG_s) for the spreading of PA from a 3D solid to 2D monolayer.[24] The equations are expressed below

$$\Delta H_s = NA_e\left\{T\left(\frac{d\pi_e}{dT}\right) - \pi_e\right\} \quad (1)$$

https://doi.org/10.1021/acsearthspacechem.2c00063
ACS Earth Space Chem. XXXX, XXX, XXX−XXX

Table 1. Calculated Thermodynamic Values of ΔH_s, ΔS_s, and ΔG_s for the 3D to 2D Spontaneous Spreading of PA on Water, 1, 10, 100, and 1000 mM NaCl Solutions at Variable Temperatures

system	T (K)	ΔH_s (kJ/mol)	ΔS_s (J/(mol·K))	ΔG_s (kJ/mol)
water	293.35 ± 1	17.35 ± 0.02	63.27 ± 0.05	−1.208 ± 0.002
	289.45 ± 1	17.50 ± 0.08	63.76 ± 0.29	−0.9529 ± 0.007
	286.05 ± 1	17.67 ± 0.07	64.57 ± 0.22	−0.8002 ± 0.011
	280.15 ± 1	18.76 ± 0.17	68.35 ± 0.59	−0.3845 ± 0.012
1 mM	293.35 ± 1	16.56 ± 0.05	60.91 ± 0.12	−1.306 ± 0.001
	289.45 ± 1	16.67 ± 0.08	61.34 ± 0.17	−1.086 ± 0.032
	286.05 ± 1	17.28 ± 0.02	63.45 ± 0.15	−0.8675 ± 0.191
	280.15 ± 1	17.56 ± 0.09	64.61 ± 0.25	−0.5438 ± 0.025
10 mM	293.35 ± 1	18.66 ± 0.08	68.83 ± 0.25	−1.536 ± 0.006
	289.45 ± 1	18.72 ± 0.09	69.35 ± 0.30	−1.348 ± 0.022
	286.05 ± 1	19.19 ± 0.07	70.81 ± 0.14	−1.069 ± 0.045
	280.15 ± 1	19.74 ± 0.08	72.90 ± 0.28	−0.6867 ± 0.012
100 mM	293.35 ± 1	15.01 ± 0.06	57.96 ± 0.15	−1.989 ± 0.034
	289.45 ± 1	15.19 ± 0.05	58.50 ± 0.10	−1.747 ± 0.022
	286.05 ± 1	15.82 ± 0.12	61.12 ± 0.38	−1.668 ± 0.016
	280.15 ± 1	16.02 ± 0.14	61.81 ± 0.43	−1.291 ± 0.018
1000 mM	293.35 ± 1	22.88 ± 0.36	89.84 ± 1.30	−3.472 ± 0.004
	289.45 ± 1	22.74 ± 0.93	90.06 ± 0.31	−3.298 ± 0.020
	286.05 ± 1	22.98 ± 0.07	90.19 ± 0.22	−2.819 ± 0.012
	280.15 ± 1	24.26 ± 0.10	95.50 ± 0.33	−2.498 ± 0.031

$$\Delta S_s = NA_e\left(\frac{d\pi_e}{dT}\right) \quad (2)$$

$$\Delta G_s = \Delta H_s - T\Delta S_s \quad (3)$$

where A_e is the mean molecular area of the monolayer (MMA) at the corresponding ESP surface pressure (converted to cm^2/molecule), N is Avogadro's number, π_e is the ESP value (expressed as dyne/cm), $\frac{d\pi_e}{dT}$ is the slope of the ESP values of a chemical system at varying temperatures (derived from Figure 3), and T is the temperature (K).

Table 1 and Figure S4 include the calculated values for changes in enthalpy (ΔH_s), entropy (ΔS_s), and Gibb's free energy (ΔG_s) for the 3D to 2D spreading of PA on different solutions at varying temperatures. As the temperature decreases within each chemical system, the ΔH_s and ΔS_s values become more positive. Colder temperatures reduce the molecular motion of PA and require more energy to spread from a 3D (polycrystalline) solid to a 2D monolayer state, resulting in a more positive enthalpy. Due to the energetic requirement to resist spreading to the 2D monolayer at cooler conditions and maintain the more ordered 3D solid-phase state, entropy increases at cooler conditions and favors the transition to the more favored and disordered 2D monolayer. In some ways, this is counterintuitive, yet one needs to consider the full chemical system, hydrating water molecules, the salt solute, and the monolayer molecules throughout the transition from 3D to 2D phase state. At colder temperatures, the equilibrium is pushed toward the 3D solid-phase state making the thermodynamic properties of spreading to the 2D monolayer less favorable. The melting point of PA is 62.9 °C.[37] Because PA is a solid throughout our temperature studies ranging from 7.0 to 20.2 °C, it is also reasonable that PA would exhibit positive ΔH_s and ΔS_s changes. Fatty acids such as oleic acid, however, have measured negative ΔH_s and ΔS_s changes, yielding highly favorable spreading from 3D solid to the 2D monolayer phase state, as oleic acid is a liquid until its melting temperature of 13.4 °C.[24] Additionally, we see that the ΔG_s is negative for all temperatures and solutions. This means that each condition will result in a 2D monolayer spreading spontaneously from the 3D solid upon deposition. Within each chemical system, however, ΔG_s becomes less negative as the temperature cools, suggesting that the 3D to 2D PA spreading is becoming less spontaneous. As the temperature approaches freezing conditions, ΔG_s approaches zero, meaning that the system exists in equilibrium.

When comparing our thermodynamic values of 3D to 2D PA spreading to literature values, we see strong agreement for pure water conditions at similar temperatures.[15,24] 3D to 2D PA spreading on pure water at 20 °C was reported as ΔH_s of 20.66 kJ/mol, ΔS_s of 74.89 J/(mol·K), and ΔG_s of −1.25 kJ/mol for the liquid condensed region.[15] Our thermodynamic values of 3D to 2D PA spreading are of the same magnitude. Our results for 3D to 2D PA spreading on pure water at 20.2 °C measure a ΔH_s of 17.35 ± 0.016 kJ/mol, ΔS_s of 63.27 ± 0.053 J/(mol·K), and ΔG_s of −1.208 ± 0.0022 kJ/mol for the liquid condensed region. While our other temperature conditions are cooler than most reported literature values, we see similar agreement for the 20 °C, suggesting a valid approach for monitoring other temperatures and subphases.

Considering other literature on similar fatty acids, differences in acyl chain length have been found to greatly influence the thermodynamic values of 3D to 2D spreading. The reported ΔH_s for stearic acid spread on pure water at 25 and 5 °C at ESP is 69.87 and 77.40 kJ/mol, respectively.[24] With the addition of two carbons in the acyl chain compared to PA, stearic acid exhibits significantly stronger dispersion forces, pushing the equilibrium to the 3D solid phase and lessening the enthalpic favorability of 3D to 2D spreading. While our ΔG_s values for PA are consistently negative, suggesting spontaneous spreading, reports from Jalal et al. calculated the ΔG_s values for the longer chained stearic acid to be positive, suggesting the dominance of the 3D solid.[24]

The trends across NaCl solutions are more complex and anomalous. Considering the NaCl systems in Table 1, as NaCl concentration increases, there is a general increase in ΔH_s.

https://doi.org/10.1021/acsearthspacechem.2c00063
ACS Earth Space Chem. XXXX, XXX, XXX−XXX

Table 2. Calculated Thermodynamic Values of $\Delta\Delta H_{PA\text{-}Na^+}$, $\Delta\Delta S_{PA\text{-}Na^+}$, and $\Delta\Delta G_{Pa\text{-}Na^+}$ for PA−Na^+ Interactions on Water, 1, 10, 100, and 1000 mM NaCl Solutions at Variable Temperatures

system	T (K)	$\Delta\Delta H_{PA\text{-}Na^+}$ (kJ/mol)	$\Delta\Delta S_{PA\text{-}Na^+}$ (J/(mol·K))	$\Delta\Delta G_{PA\text{-}Na^+}$ (kJ/mol)
1 mM	293.35 ± 1	−0.79 ± 0.05	−2.36 ± 0.13	−0.0984 ± 0.01
	289.45 ± 1	−0.83 ± 0.11	−2.42 ± 0.33	−0.133 ± 0.03
	286.05 ± 1	−0.39 ± 0.08	−1.12 ± 0.26	−0.0673 ± 0.03
	280.15 ± 1	−1.21 ± 0.19	−3.74 ± 0.64	−0.159 ± 0.03
10 mM	293.35 ± 1	1.30 ± 0.08	5.56 ± 0.26	−0.329 ± 0.01
	289.45 ± 1	1.22 ± 0.12	5.59 ± 0.41	−0.395 ± 0.02
	286.05 ± 1	1.52 ± 0.10	6.24 ± 0.26	−0.269 ± 0.05
	280.15 ± 1	0.97 ± 0.19	4.54 ± 0.65	−0.302 ± 0.02
100 mM	293.35 ± 1	−2.34 ± 0.06	−5.31 ± 0.16	−0.781 ± 0.03
	289.45 ± 1	−2.32 ± 0.09	−5.26 ± 0.30	−0.794 ± 0.02
	286.05 ± 1	−1.85 ± 0.14	−3.45 ± 0.44	−0.868 ± 0.02
	280.15 ± 1	−2.74 ± 0.22	−6.54 ± 0.73	−0.907 ± 0.03
1000 mM	293.35 ± 1	5.53 ± 0.36	26.57 ± 1.27	−2.27 ± 0.04
	289.45 ± 1	5.24 ± 0.12	26.3 ± 0.42	−2.38 ± 0.03
	286.05 ± 1	5.31 ± 0.11	25.62 ± 0.22	−2.01 ± 0.02
	280.15 ± 1	5.49 ± 0.20	27.15 ± 0.68	−2.11 ± 0.04

Work by Wellen Rudd et al. similarly summarizes trends in thermodynamic properties for 3D to 2D PA spreading on NaCl solutions, showing an increase in ESP and ΔH_s due to the induced charge Na^+ presents to a closely packed PA monolayer.[14,38] However, when considering the 100 mM NaCl system, we observe the least positive values in ΔH_s, or a slight increase in enthalpic favorability, falling out of trend with the other NaCl systems, which are all more positive in value.

Previous work by Adams et al. details the favorable conditions 100 mM NaCl poses in driving PA to the air−water interface in the 2D phase state.[25] For the 100 mM NaCl solution, metal ions have been shown via infrared reflection-absorption spectroscopy to alter the hydration of the carboxylate headgroups.[2,27,30,39] The PA headgroup can undergo two types of Na^+ coordination, either binding to one oxygen or both oxygen atoms of the PA headgroup. Spatial distribution functions were reported in literature explaining these potential sodium interactions with PA.[25] It has been shown that PA interacts with one or two Na^+, and these differences in coordination could elucidate the anomalous thermodynamic values of 3D to 2D spreading we are observing in the 100 mM NaCl system.

From eqs 1 to 3, we calculated the thermodynamic values of 3D to 2D spreading of PA. We can extend these values to a new thermodynamic interpretation of PA−Na^+ interaction by subtracting the pure water thermodynamic properties of spreading from the NaCl systems. By assuming a constant hydration environment for all pure water conditions, we determined the direct thermodynamic values of PA−Na^+ interaction.

Thermodynamic Properties of Palmitic Acid−Sodium Ion Interactions at the Air−Water Interface. Other studies have calculated the thermodynamic properties of 3D to 2D spreading for PA on different salt solutions,[15,16,24,34,40] but none have considered the thermodynamic properties of carboxylate−metal interactions for proxy SSA interfaces. However, carboxylate−metal interactions such as contact ion pairing and solvent sharing have been well documented by spectroscopic investigation,[41,42] demonstrating a need for further thermodynamic elucidation.[6,30,34,39,43−47] Therefore, we can exploit our ESP values to obtain the thermodynamic properties of PA−Na^+ interactions given the following equations. The enthalpy ($\Delta\Delta H_{PA\text{-}Na^+}$), entropy ($\Delta\Delta S_{PA\text{-}Na^+}$), and Gibb's free energy ($\Delta\Delta G_{PA\text{-}Na^+}$) of PA−$Na^+$ interactions can be calculated using eqs 4−6.

$$\Delta\Delta H_{PA-Na^+} = \Delta H_{spreading,water,NaCl} - \Delta H_{spreading,water} \quad (4)$$

$$\Delta\Delta S_{PA-Na^+} = \Delta S_{spreading,water,NaCl} - \Delta S_{spreading,water} \quad (5)$$

$$\Delta\Delta G_{PA-Na^+} = \Delta G_{spreading,water,NaCl} - \Delta G_{spreading,water} \quad (6)$$

Our PA and NaCl model system is only one example of this, but this approach could be applied to other atmospherically relevant systems. Herein, we calculate the first thermodynamic values of PA−Na^+ intermolecular interactions at a range of temperatures and NaCl concentrations, as presented in Table 2.

Similar to Table 1, the 100 mM NaCl system diverges from a monotonical trend with the other NaCl solutions regarding the thermodynamic properties of PA−Na^+ interactions. The 1 mM NaCl and 100 mM systems are both negative in $\Delta\Delta H_{PA\text{-}Na^+}$, $\Delta\Delta S_{PA\text{-}Na^+}$, suggesting that these Na^+ concentrations are most favorable for carboxylate−metal interactions. All NaCl solutions exhibit negative $\Delta\Delta G_{PA\text{-}Na^+}$, showing the PA−$Na^+$ interactions to be spontaneous. However, the 1 M NaCl system yields the most positive $\Delta\Delta H_{PA\text{-}Na^+}$ due to the unfavorable electrostatic repulsion of the remaining 3D solid phase of PA. To mitigate these unfavorable interactions in the 3D phase state, we observe the most spontaneous interactions with the 2D monolayer of PA, as demonstrated by the most negative $\Delta\Delta G_{PA-Na^+}$.

Atmospheric Significance. Fatty acids are enriched on the surface of sea spray aerosols (SSAs).[48−54] SSAs, which are formed upon wave breaking processes through bubble entrainment then bursting at the air−seawater interface,[55−57] are a major contributor to the total global aerosol mass.[48,52,58,59] Additionally, the ocean concentration of sodium chloride is ∼0.45 M.[60] Given atmospheric conditions, such as relative humidity, the sodium chloride concentration can become dilute (Figure 5) and exhibit 100 mM NaCl concentrations, which were found to be thermodynamically favorable for 2D monolayer phase-state maintenance. These marine aerosols are an important input in climate models as they impact the earth's radiative balance through interactions

https://doi.org/10.1021/acsearthspacechem.2c00063
ACS Earth Space Chem. XXXX, XXX, XXX−XXX

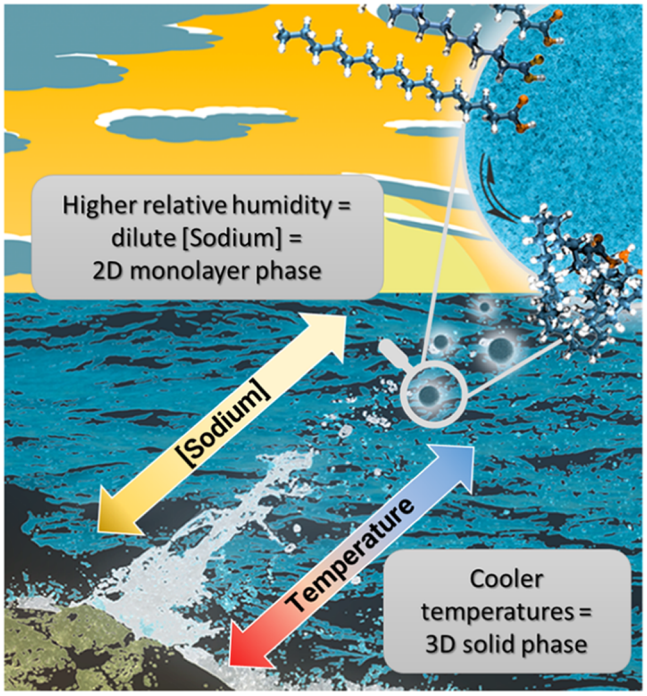

Figure 5. Schematic depiction of how atmospheric conditions of temperature and sodium concentration are driving the phase-state equilibrium of palmitic acid. As relative humidity dilutes the concentration of sodium, the phase state is pushed to the 2D monolayer state. As temperatures cool at higher altitudes, the phase state is pushed to the 3D solid state. An interplay of both atmospheric conditions results in highly dynamic phase states of molecules at the aerosol interface.

with solar radiation and serve as cloud condensation and ice nuclei.[61,62] Previous work by Cochran et al. showed that palmitic and stearic acid comprised two-thirds of the total ion signal of identified saturated fatty acids of SSA particles collected from the ocean.[54] Studies that followed showed that the PA−Na^+ interactions help stabilize the air−water interface.[2,34]

Additionally, fatty acids like PA have been abundantly sourced from marine algae,[63] undergo temporal fluctuations in enrichment at the air−seawater interface,[64] and contribute to ice nucleating particle (INP) counts.[35,65,66] According to McCluskey et al., long chain fatty acids can be active INPs at −30 °C.[65] Additionally, ESP has been used as a tool for thermodynamic consideration pertaining to ice nucleation.[21] As temperatures decrease at higher altitudes due to changes in pressure,[67] fatty acid monolayers undergo a decrease in ESP and increase in mean molecular area (MMA). The increase in MMA is defined by Perkins et al. as the maximum MMA, or max-MMA_{eq}, that the monolayer exists for a given ESP and temperature. Max-MMA_{eq} for colder temperatures means a less compact monolayer as fatty acid material partitions and equilibrates to the 3D solid-phase state.[21] This partitioning is thermodynamically favorable for certain ice processes as the 3D solid phase can provide a site for nucleation.[68,69] Recent findings from Mael et al. calculate several ice nucleation thermodynamics of micron-sized droplets containing biologically and marine relevant atmospheric inclusions with consideration of oceanic salt concentrations as a function of temperature.[70] Thermodynamic evaluation of the interfacial phase state of organic coatings is important for clarifying different atmospheric phenomena but still persists as a fundamental question many scientists are working to address.[71−73] Phase-state equilibrium remains highly relevant to our global understanding of aerosol interfaces, and our approach to calculating the thermodynamic properties of carboxylate−metal interactions on SSA surfaces helps to unravel the complexity of interfacial and atmospheric chemistry.

CONCLUSIONS

Equilibrium spreading pressure (ESP) measurements are representative of a true state of thermodynamic equilibrium at the aqueous surface. As temperatures become colder, the ESP values decrease across all chemical solutions (water, 1, 10, 100, and 1000 mM NaCl). The 3D to 2D spreading for palmitic acid is overall spontaneous at all temperatures studied with and without NaCl added to the solutions. The enthalpic and entropic contributions are shown to be positive, pointing to the dominance of the $-T\Delta S$ term in determining the persistently negative Gibb's free energy for the 3D to 2D transition. Cooler temperatures present less negative Gibb's free energy values or less spontaneous thermodynamic conditions, for 3D solid to 2D monolayer spreading of PA. However, the addition of NaCl to the solution does not follow a monotonical trend in enthalpy and entropy values of 3D to 2D spreading, specifically exhibited by an anomalous 100 mM NaCl condition which is ∼20 and ∼35% more enthalpically favorable than 10 and 1000 mM NaCl solutions, respectively. Thermodynamic properties of carboxylate−metal interactions were calculated for all NaCl systems, and the 1 M NaCl results were the most negative in $\Delta\Delta G_{PA\text{-}Na^+}$, suggesting a more spontaneous system for interacting. To the authors' knowledge, this is the first report on using measured ESP values for calculating the thermodynamic equilibrium of PA−Na^+ interactions for proxy SSA interfaces. Future investigation is needed to apply this approach to more dynamic systems to determine the feasibility of such a straightforward technique for complex calculations and models.

ASSOCIATED CONTENT

Supporting Information

The Supporting Information is available free of charge at https://pubs.acs.org/doi/10.1021/acsearthspacechem.2c00063.

Equilibrium spreading pressure of ethylenediaminetetraacetic acid, schematic representation of calculating thermodynamics values from experimental equilibrium spreading pressure and Π-A isotherms, Π-A isotherms for palmitic acid on 0, 1, 10, 100, and 1000 mM NaCl subphases organized by temperature, and thermodynamics of spreading palmitic acid on 0, 1, 10, 100, and 1000 mM NaCl subphases plotted (PDF)

AUTHOR INFORMATION

Corresponding Author

Heather C. Allen − *Department of Chemistry & Biochemistry, The Ohio State University, Columbus, Ohio 43210, United States;* orcid.org/0000-0003-3120-6784; Email: allen@chemistry.ohio-state.edu

https://doi.org/10.1021/acsearthspacechem.2c00063
ACS Earth Space Chem. XXXX, XXX, XXX−XXX

Authors

Mickey M. Rogers − *Department of Chemistry & Biochemistry, The Ohio State University, Columbus, Ohio 43210, United States*

Maria G. Vazquez de Vasquez − *Department of Chemistry & Biochemistry, The Ohio State University, Columbus, Ohio 43210, United States*

Jennifer F. Neal − *Department of Chemistry & Biochemistry, The Ohio State University, Columbus, Ohio 43210, United States*

Mia M. Zerkle − *Department of Chemistry & Biochemistry, The Ohio State University, Columbus, Ohio 43210, United States*

Brittany M. Shook − *Department of Chemistry & Biochemistry, The Ohio State University, Columbus, Ohio 43210, United States*

Complete contact information is available at: https://pubs.acs.org/10.1021/acsearthspacechem.2c00063

Author Contributions

M.M.R. and J.F.N. designed the study. M.M.R., M.G.V.d.V., M.M.Z., and B.M.S. collected all data. M.M.R. and M.G.V.d.V. processed experimental data. J.F.N. assisted on data conceptualization and discussion. M.M.R., M.G.V.d,V. and J.F.N. wrote and edited the manuscript. H.C.A. edited the manuscript and supervised the study.

Notes

The authors declare no competing financial interest.

■ ACKNOWLEDGMENTS

J.F.N., M.M.Z., and B.M.S. acknowledge support by the National Science Foundation (NSF) MSN program, CHE-1609672. M.M.R. and M.G.V.d.V. acknowledge support by the NSF through the Center for Aerosol Impacts on Chemistry of the Environment (CAICE), CHE-1801971. Data archiving is underway at the UC San Diego Library Digital Collections for CAICE website: https://doi.org/10.6075/J0NC61CR. The authors declare no competing financial interest. The authors would like to thank B. Rogers, B. Vasquez, R.B. Vazquez, Dr. L. Mael, Dr. K. Carter-Fenk, and A. Fonlon for valuable input and review.

■ REFERENCES

(1) Auvil, N. C.; Vazquez de Vasquez, M. G.; Allen, H. C. Zinc−Carboxylate Binding in Mixed Octadecanoic Acid and Octadecanol Monolayers on Proxy Seawater Solution Surfaces. *ACS Earth Space Chem.* **2021**, *5*, 2947−2956.

(2) Vazquez de Vasquez, M. G.; Wellen Rudd, B. A.; Baer, M. D.; Beasley, E. E.; Allen, H. C. Role of Hydration in Magnesium versus Calcium Ion Pairing with Carboxylate: Solution and the Aqueous Interface. *J. Phys. Chem. B* **2021**, *125*, 11308−11319.

(3) Neal, J. F.; Rogers, M. M.; Smeltzer, M. A.; Carter-Fenk, K. A.; Grooms, A. J.; Zerkle, M. M.; Allen, H. C. Sodium Drives Interfacial Equilibria for Semi-Soluble Phosphoric and Phosphonic Acids of Model Sea Spray Aerosol Surfaces. *ACS Earth Space Chem.* **2020**, *4*, 1549−1557.

(4) Wellen, B. A.; Lach, E. A.; Allen, H. C. Surface PKa of Octanoic, Nonanoic, and Decanoic Fatty Acids at the Air−Water Interface: Applications to Atmospheric Aerosol Chemistry. *Phys. Chem. Chem. Phys.* **2017**, *19*, 26551−26558.

(5) Griffith, E. C.; Vaida, V. Ionization State of L-Phenylalanine at the Air−Water Interface. *J. Am. Chem. Soc.* **2013**, *135*, 710−716.

(6) Allen, H. C.; Casillas-Ituarte, N. N.; Sierra-Hernández, M. R.; Chen, X.; Tang, C. Y. Shedding Light on Water Structure at Air−Aqueous Interfaces: Ions, Lipids, and Hydration. *Phys. Chem. Chem. Phys.* **2009**, *11*, 5538−5549.

(7) Neal, J. F. *Molecular Recognition of Organic and Inorganic Phosphates at the Aqueous Interface*, The Ohio State University, 2020.

(8) Ariga, K. Molecular Recognition at the Air−Water Interface: Nanoarchitectonic Design and Physicochemical Understanding. *Phys. Chem. Chem. Phys.* **2020**, *22*, 24856−24869.

(9) Mansour, H. M.; Zografi, G. Relationships between Equilibrium Spreading Pressure and Phase Equilibria of Phospholipid Bilayers and Monolayers at the Air-Water Interface. *Langmuir* **2007**, *23*, 3809−3819.

(10) Sulthana, S. B.; Bhat, S. G. T.; Rakshit, A. K. Thermodynamics of Micellization of a Non-Ionic Surfactant Myrj 45: Effect of Additives. *Colloids Surf., A* **1996**, *111*, 57−65.

(11) Gaines, G. L. *Insoluble Monolayers at Liquid-Gas Interfaces*; Interscience Publishers: New York, 1966.

(12) Oliveira, O. N.; Caseli, L.; Ariga, K. The Past and the Future of Langmuir and Langmuir−Blodgett Films. *Chem. Rev.* **2022**, *122*, 6459−6513.

(13) Motomura, K.; Yoshino, S.; Fujii, K.; Matuura, R. Thermodynamics of Multicomponent Monolayers: III. Equilibrium Spreading Pressure of Two-Component Mixtures. *J. Colloid Interface Sci.* **1977**, *60*, 87−95.

(14) Wellen Rudd, B. A.; Vidalis, A. S.; Allen, H. C. Thermodynamic versus Non-Equilibrium Stability of Palmitic Acid Monolayers in Calcium-Enriched Sea Spray Aerosol Proxy Systems. *Phys. Chem. Chem. Phys.* **2018**, *20*, 16320−16332.

(15) Boyd, G. E. Energy Relations in Monolayer Formation: The Spreading of Long-Chain Fatty Acids on Aqueous Surfaces. *J. Phys. Chem. A* **1958**, *62*, 536−541.

(16) Boyd, G. E.; Schubert, J. Energy Relations in Unimolecular Film Formation: The Spreading of Cetyl Alcohol and Palmitic Acid on Aqueous Surfaces. *J. Phys. Chem. B* **1957**, *61*, 1271−1275.

(17) Phillips, M. C.; Hauser, H. Spreading of Solid Glycerides and Phospholipids at the Air—Water Interface. *J. Colloid Interface Sci.* **1974**, *49*, 31−39.

(18) Niño, M. R. R.; Sánchez, C. C.; Fernández, M. C.; Patino, J. M. R. Protein and Lipid Films at Equilibrium at Air-Water Interface. *J. Am. Oil Chem. Soc.* **2001**, *78*, 873−879.

(19) Rettig, W.; Kuschel, F. A First-Order Transition between the Liquid-Expanded and the Liquid-Condensed Phases in Insoluble Monolayers of Fatty Acid Esters as Detected by Measurement of Equilibrium Spreading Pressure. *J. Colloid Interface Sci.* **1990**, *140*, 169−174.

(20) Knopf, D. A.; Forrester, S. M. Freezing of Water and Aqueous NaCl Droplets Coated by Organic Monolayers as a Function of Surfactant Properties and Water Activity. *J. Phys. Chem. A* **2011**, *115*, 5579−5591.

(21) Perkins, R. J.; Vazquez de Vasquez, M. G.; Beasley, E. E.; Hill, T. C. J.; Stone, E. A.; Allen, H. C.; DeMott, P. J. Relating Structure and Ice Nucleation of Mixed Surfactant Systems Relevant to Sea Spray Aerosol. *J. Phys. Chem. A* **2020**, *124*, 8806−8821.

(22) Qiu, Y.; Odendahl, N.; Hudait, A.; Mason, R.; Bertram, A. K.; Paesani, F.; DeMott, P. J.; Molinero, V. Ice Nucleation Efficiency of Hydroxylated Organic Surfaces Is Controlled by Their Structural Fluctuations and Mismatch to Ice. *J. Am. Chem. Soc.* **2017**, *139*, 3052−3064.

(23) Neal, J. F.; Zhao, W.; Grooms, A. J.; Flood, A. H.; Allen, H. C. Arginine−Phosphate Recognition Enhanced in Phospholipid Monolayers at Aqueous Interfaces. *J. Phys. Chem. C* **2018**, *122*, 26362−26371.

(24) Jalal, I. M.; Zografi, G.; Rakshit, A. K.; Gunstone, F. D. Monolayer Properties of Fatty Acids. I. Thermodynamics of Spreading. *J. Colloid Interface Sci.* **1980**, *76*, 146−156.

(25) Adams, E. M.; Wellen, B. A.; Thiraux, R.; Reddy, S. K.; Vidalis, A. S.; Paesani, F.; Allen, H. C. Sodium−Carboxylate Contact Ion Pair Formation Induces Stabilization of Palmitic Acid Monolayers at High PH. *Phys. Chem. Chem. Phys.* **2017**, *19*, 10481−10490.

(26) Council (U.S.), N. R. *International Critical Tables of Numerical Data, Physics, Chemistry and Technology*; National research council, 1926.
(27) Vidalis, A. The Stability of Palmitic Acid Monolayers. Thesis, The Ohio State University, 2017.
(28) Lipp, M. M.; Lee, K. Y.; Waring, A.; Zasadzinski, J. A. Fluorescence, Polarized Fluorescence, and Brewster Angle Microscopy of Palmitic Acid and Lung Surfactant Protein B Monolayers. *Biophys. J.* **1997**, *72*, 2783−2804.
(29) Carter-Fenk, K. A.; Allen, H. C. Collapse Mechanisms of Nascent and Aged Sea Spray Aerosol Proxy Films. *Atmosphere* **2018**, *9*, 503.
(30) Tang, C. Y.; Allen, H. C. Ionic Binding of Na+ versus K+ to the Carboxylic Acid Headgroup of Palmitic Acid Monolayers Studied by Vibrational Sum Frequency Generation Spectroscopy. *J. Phys. Chem. A* **2009**, *113*, 7383−7393.
(31) Heikkila, R. E.; Kwong, C. N.; Cornwell, D. G. Stability of Fatty Acid Monolayers and the Relationship between Equilibrium Spreading Pressure, Phase Transformations, and Polymorphic Crystal Forms. *J. Lipid Res.* **1970**, *11*, 190−194.
(32) Broniatowski, M.; Dynarowicz-Łątka, P.; Camacho, L.; Martin Romero, M. T.; Muñoz, E. Semifluorinated Thiols in Langmuir Monolayers. *J. Colloid Interface Sci.* **2010**, *346*, 153−162.
(33) Broniatowski, M. Long-Chain Alkyl Thiols in Langmuir Monolayers. *J. Colloid Interface Sci.* **2009**, *337*, 183−190.
(34) Adams, E. M.; Wellen, B. A.; Thiraux, R.; Reddy, S. K.; Vidalis, A. S.; Paesani, F.; Allen, H. C. Sodium-Carboxylate Contact Ion Pair Formation Induces Stabilization of Palmitic Acid Monolayers at High PH. *Phys. Chem. Chem. Phys.* **2017**, *19*, 10481−10490.
(35) DeMott, P. J.; Mason, R. H.; McCluskey, C. S.; Hill, T. C. J.; Perkins, R. J.; Desyaterik, Y.; Bertram, A. K.; Trueblood, J. V.; Grassian, V. H.; Qiu, Y.; Molinero, V.; Tobo, Y.; Sultana, C. M.; Lee, C.; Prather, K. A. Ice Nucleation by Particles Containing Long-Chain Fatty Acids of Relevance to Freezing by Sea Spray Aerosols. *Environ. Sci.: Processes Impacts* **2018**, *20*, 1559−1569.
(36) Pashkovskaya, A. A.; Vazdar, M.; Zimmermann, L.; Jovanovic, O.; Pohl, P.; Pohl, E. E. Mechanism of Long-Chain Free Fatty Acid Protonation at the Membrane-Water Interface. *Biophys. J.* **2018**, *114*, 2142−2151.
(37) Beare-Rogers, J. L.; Dieffenbacher, A.; Holm, J. V. Lexicon of lipid nutrition (IUPAC Technical Report). *Pure Appl. Chem.* **2001**, *73*, 685−744.
(38) Prpich, A. M.; Sheng, Y.; Wang, W.; Biswas, M. E.; Chen, P. Tension at the Surface: Which Phase Is More Important, Liquid or Vapor? *PLoS One* **2009**, *4*, No. e8281.
(39) Wellen Rudd, B. A.; Vidalis, A. S.; Allen, H. C. Thermodynamic versus Non-Equilibrium Stability of Palmitic Acid Monolayers in Calcium-Enriched Sea Spray Aerosol Proxy Systems. *Phys. Chem. Chem. Phys.* **2018**, *20*, 16320−16332.
(40) Pogorzelski, S. J.; Rochowski, P.; Grzegorczyk, M.; Boniewicz-Szmyt, K. Snowpack-Stored Atmospheric Surface-Active Contaminants Traced with Snowmelt Water Surface Film Rheology. *Environ. Sci. Pollut. Res.* **2021**, *28*, 5443−5454.
(41) Huang, Z.; Hua, W.; Verreault, D.; Allen, H. C. Influence of Salt Purity on Na+ and Palmitic Acid Interactions. *J. Phys. Chem. A* **2013**, *117*, 13412−13418.
(42) Sthoer, A.; Tyrode, E. Interactions of Na+ Cations with a Highly Charged Fatty Acid Langmuir Monolayer: Molecular Description of the Phase Transition. *J. Phys. Chem. C* **2019**, *123*, 23037−23048.
(43) Shrestha, M.; Luo, M.; Li, Y.; Xiang, B.; Xiong, W.; Grassian, V. H. Let There Be Light: Stability of Palmitic Acid Monolayers at the Air/Salt Water Interface in the Presence and Absence of Simulated Solar Light and a Photosensitizer. *Chem. Sci.* **2018**, *9*, 5716−5723.
(44) Hua, W.; Verreault, D.; Huang, Z.; Adams, E. M.; Allen, H. C. Cation Effects on Interfacial Water Organization of Aqueous Chloride Solutions. I. Monovalent Cations: Li+, Na+, K+, and NH4+. *J. Phys. Chem. B* **2014**, *118*, 8433−8440.
(45) Le Calvez, E.; Blaudez, D.; Buffeteau, T.; Desbat, B. Effect of Cations on the Dissociation of Arachidic Acid Monolayers on Water Studied by Polarization-Modulated Infrared Reflection−Absorption Spectroscopy. *Langmuir* **2001**, *17*, 670−674.
(46) Sam, S.; Krem, S.; Lee, J.; Kim, D. Recovery of Fatty Acid Monolayers by Salts Investigated by Sum-Frequency Generation Spectroscopy. *J. Phys. Chem. B* **2022**, *126*, 643−649.
(47) Foster, M. J.; Carpenter, A. P.; Richmond, G. L. Dynamic Duo: Vibrational Sum Frequency Scattering Investigation of PH-Switchable Carboxylic Acid/Carboxylate Surfactants on Nanodroplet Surfaces. *J. Phys. Chem. B* **2021**, *125*, 9629−9640.
(48) Quinn, P. K.; Collins, D. B.; Grassian, V. H.; Prather, K. A.; Bates, T. S. Chemistry and Related Properties of Freshly Emitted Sea Spray Aerosol. *Chem. Rev.* **2015**, *115*, 4383−4399.
(49) Donaldson, D. J.; George, C. Sea-Surface Chemistry and Its Impact on the Marine Boundary Layer. *Environ. Sci. Technol.* **2012**, *46*, 10385−10389.
(50) Wang, X.; Sultana, C. M.; Trueblood, J.; Hill, T. C. J.; Malfatti, F.; Lee, C.; Laskina, O.; Moore, K. A.; Beall, C. M.; McCluskey, C. S.; Cornwell, G. C.; Zhou, Y.; Cox, J. L.; Pendergraft, M. A.; Santander, M. V.; Bertram, T. H.; Cappa, C. D.; Azam, F.; DeMott, P. J.; Grassian, V. H.; Prather, K. A. Microbial Control of Sea Spray Aerosol Composition: A Tale of Two Blooms. *ACS Cent. Sci.* **2015**, *1*, 124−131.
(51) Burrows, S. M.; Ogunro, O.; Frossard, A. A.; Russell, L. M.; Rasch, P. J.; Elliott, S. M. A Physically Based Framework for Modeling the Organic Fractionation of Sea Spray Aerosol from Bubble Film Langmuir Equilibria. *Atmos. Chem. Phys.* **2014**, *14*, 13601−13629.
(52) Gantt, B.; Nicholas, M. The Physical and Chemical Characteristics of Marine Primary Organic Aerosol: A Review. *Atmos. Chem. Phys.* **2013**, *13*, 3979−3996.
(53) Schmitt-Kopplin, P.; Liger-Belair, G.; Koch, B. P.; Flerus, R.; Kattner, G.; Harir, M.; Kanawati, B.; Lucio, M.; Tziotis, D.; Hertkorn, N.; Gebefügi, I. Dissolved Organic Matter in Sea Spray: A Transfer Study from Marine Surface Water to Aerosols. *Biogeosciences* **2012**, *9*, 1571−1582.
(54) Cochran, R. E.; Laskina, O.; Jayarathne, T.; Laskin, A.; Laskin, J.; Lin, P.; Sultana, C.; Lee, C.; Moore, K. A.; Cappa, C. D.; Bertram, T. H.; Prather, K. A.; Grassian, V. H.; Stone, E. A. Analysis of Organic Anionic Surfactants in Fine and Coarse Fractions of Freshly Emitted Sea Spray Aerosol. *Environ. Sci. Technol.* **2016**, *50*, 2477−2486.
(55) Prather, K. A.; Bertram, T. H.; Grassian, V. H.; Deane, G. B.; Stokes, M. D.; DeMott, P. J.; Aluwihare, L. I.; Palenik, B. P.; Azam, F.; Seinfeld, J. H.; Moffet, R. C.; Molina, M. J.; Cappa, C. D.; Geiger, F. M.; Roberts, G. C.; Russell, L. M.; Ault, A. P.; Baltrusaitis, J.; Collins, D. B.; Corrigan, C. E.; Cuadra-Rodriguez, L. A.; Ebben, C. J.; Forestieri, S. D.; Guasco, T. L.; Hersey, S. P.; Kim, M. J.; Lambert, W. F.; Modini, R. L.; Mui, W.; Pedler, B. E.; Ruppel, M. J.; Ryder, O. S.; Schoepp, N. G.; Sullivan, R. C.; Zhao, D. F. Bringing the Ocean into the Laboratory to Probe the Chemical Complexity of Sea Spray Aerosol. *Proc. Natl. Acad. Sci. U.S.A.* **2013**, *110*, 7550.
(56) Callaghan, A. H.; Stokes, M. D.; Deane, G. B. The Effect of Water Temperature on Air Entrainment, Bubble Plumes, and Surface Foam in a Laboratory Breaking-Wave Analog. *J. Geophys. Res.: Oceans* **2014**, *119*, 7463−7482.
(57) Collins, D. B.; Zhao, D. F.; Ruppel, M. J.; Laskina, O.; Grandquist, J. R.; Modini, R. L.; Stokes, M. D.; Russell, L. M.; Bertram, T. H.; Grassian, V. H.; Deane, G. B.; Prather, K. A. Direct Aerosol Chemical Composition Measurements to Evaluate the Physicochemical Differences between Controlled Sea Spray Aerosol Generation Schemes. *Atmos. Meas. Tech.* **2014**, *7*, 3667−3683.
(58) Frossard, A. A.; Gérard, V.; Duplessis, P.; Kinsey, J. D.; Lu, X.; Zhu, Y.; Bisgrove, J.; Maben, J. R.; Long, M. S.; Chang, R. Y.-W.; Beaupré, S. R.; Kieber, D. J.; Keene, W. C.; Nozière, B.; Cohen, R. C. Properties of Seawater Surfactants Associated with Primary Marine Aerosol Particles Produced by Bursting Bubbles at a Model Air−Sea Interface. *Environ. Sci. Technol.* **2019**, *53*, 9407−9417.
(59) Frossard, A. A.; Russell, L. M.; Burrows, S. M.; Elliott, S. M.; Bates, T. S.; Quinn, P. K. Sources and Composition of Submicron

Organic Mass in Marine Aerosol Particles. *J. Geophys. Res.: Atmos.* **2014**, *119*, 12,977−13,003.
(60) Millero, F. J. *Chemical Oceanography*, 2nd ed.; CRC Press, 1996.
(61) de Leeuw, G.; Andreas, E. L.; Anguelova, M. D.; Fairall, C. W.; Lewis, E. R.; O'Dowd, C.; Schulz, M.; Schwartz, S. E. Production Flux of Sea Spray Aerosol. *Rev. Geophys.* **2011**, *49*, No. 349.
(62) O'Dowd, C. D.; De Leeuw, G. Marine Aerosol Production: A Review of the Current Knowledge. *Philos. Trans. R. Soc., A* **2007**, *365*, 1753.
(63) Lang, I.; Hodac, L.; Friedl, T.; Feussner, I. Fatty Acid Profiles and Their Distribution Patterns in Microalgae: A Comprehensive Analysis of More than 2000 Strains from the SAG Culture Collection. *BMC Plant Biol.* **2011**, *11*, No. 124.
(64) Rogers, M. M.; Neal, J. F.; Saha, A.; Algarni, A. S.; Hill, T. C. J.; Allen, H. C. The Ocean's Elevator: Evolution of the Air−Seawater Interface during a Small-Scale Algal Bloom. *ACS Earth Space Chem.* **2020**, *4*, 2347−2357.
(65) McCluskey, C. S.; Hill, T. C. J.; Sultana, C. M.; Laskina, O.; Trueblood, J.; Santander, M. V.; Beall, C. M.; Michaud, J. M.; Kreidenweis, S. M.; Prather, K. A.; Grassian, V.; DeMott, P. J. A Mesocosm Double Feature: Insights into the Chemical Makeup of Marine Ice Nucleating Particles. *J. Atmos. Sci.* **2018**, *75*, 2405−2423.
(66) Jacquemain, D.; Leveiller, F.; Weinbach, S. P.; Lahav, M.; Leiserowitz, L.; Kjaer, K.; Als-Nielsen, J. Crystal Structure of Self-Aggregates of Insoluble Aliphatic Amphiphilic Molecules at the Air-Water Interface. An x-Ray Synchrotron Study. *J. Am. Chem. Soc.* **1991**, *113*, 7684−7691.
(67) Ohmura, A. Enhanced Temperature Variability in High-Altitude Climate Change. *Theor. Appl. Climatol.* **2012**, *110*, 499−508.
(68) Knopf, D. A.; Alpert, P. A.; Wang, B. The Role of Organic Aerosol in Atmospheric Ice Nucleation: A Review. *ACS Earth Space Chem.* **2018**, *2*, 168−202.
(69) Laskin, A.; Gilles, M. K.; Knopf, D. A.; Wang, B.; China, S. Progress in the Analysis of Complex Atmospheric Particles. *Annu. Rev. Anal. Chem.* **2016**, *9*, 117−143.
(70) Mael, L. E.; Peiker, G.; Busse, H. L.; Grassian, V. H. Temperature-Dependent Liquid Water Structure for Individual Micron-Sized, Supercooled Aqueous Droplets with Inclusions. *J. Phys. Chem. A* **2021**, *125*, 10742−10749.
(71) Altaf, M. B.; Zuend, A.; Freedman, M. A. Role of Nucleation Mechanism on the Size Dependent Morphology of Organic Aerosol. *Chem. Commun.* **2016**, *52*, 9220−9223.
(72) Losey, D. J.; Ott, E.-J. E.; Freedman, M. A. Effects of High Acidity on Phase Transitions of an Organic Aerosol. *J. Phys. Chem. A* **2018**, *122*, 3819−3828.
(73) Freedman, M. A. Phase Separation in Organic Aerosol. *Chem. Soc. Rev.* **2017**, *46*, 7694−7705.

https://doi.org/10.1021/acsearthspacechem.2c00063
ACS Earth Space Chem. XXXX, XXX, XXX−XXX